Stem Cells, 2022, **40**, 318–331
https://doi.org/10.1093/stmcls/sxab026
Advance access publication 21 January 2022
Original Research

Neural Stem Cell-Derived Extracellular Vesicles Counteract Insulin Resistance-Induced Senescence of Neurogenic Niche

Francesca Natale[1,2], Lucia Leone[1,2], Marco Rinaudo[1], Raimondo Sollazzo[1], Saviana Antonella Barbati[1], Francesco La Greca[1], Matteo Spinelli[1], Salvatore Fusco[1,2,*], Claudio Grassi[1,2]

[1]Department of Neuroscience, Università Cattolica del Sacro Cuore, Rome, Italy
[2]Fondazione Policlinico Universitario A. Gemelli IRCCS, Rome, Italy

*Corresponding author: Department of Neuroscience, 3rd floor Istituti Biologici Building, Università Cattolica del Sacro Cuore, Largo Francesco Vito 1, 00168 Rome, Italy. Tel: +39 06 3015 4966; Email: salvatore.fusco@unicatt.it

Abstract

Neural stem and progenitor cell (NSPC) depletion may play a crucial role in the cognitive impairment observed in many age-related non-communicable diseases. Insulin resistance affects brain functions through a plethora of mechanisms that remain poorly understood. In an experimental model of insulin resistant NSPCs, we identified a novel molecular circuit relying on insulin receptor substrate-1 (IRS-1)/ Forkhead box O (FoxO) signaling cascade and inhibiting the recruitment of transcription factors FoxO1 and FoxO3a on the promoters of genes regulating proliferation and self-renewal. Insulin resistance also epigenetically increased the expression of cyclin-dependent kinase inhibitor 1 (p21) and accelerated NSPC senescence. Of note, we found that stimulation of NSPCs with NSPC-derived exosomes (exo-NSPC) rescued IRS-1/FoxO activation and counteracted both the reduced proliferation and senescence of stem cells. Accordingly, intranasal administration of exo-NSPC counteracted the high-fat diet-dependent impairment of adult hippocampal neurogenesis in mice by restoring the balance between proliferating and senescent NSPCs in the hippocampus. Our findings suggest a novel mechanism underlying the metabolic control of NSPC fate potentially involved in the detrimental effects of metabolic disorders on brain plasticity. In addition, our data highlight the role of extracellular vesicle-mediated signals in the regulation of cell fate within the adult neurogenic niche.

Key words: adult neurogenesis; ageing; extracellular vesicles; neural stem cells; insulin resistance; senescence; personalized medicine.

Graphical Abstract

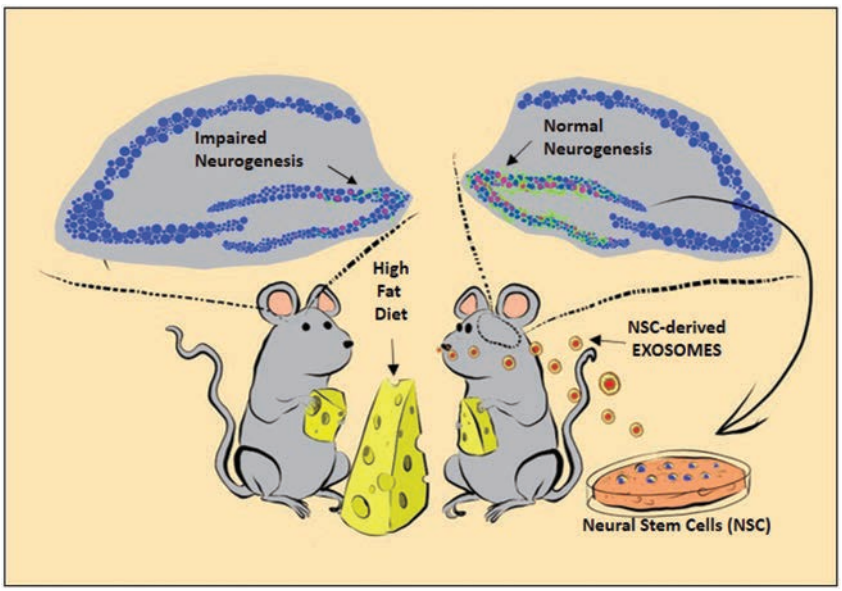

Intranasal administration of neural stem cell-derived exosomes counteract the high-fat diet-dependent depletion of hippocampal neurogenic niche.

Received: 19 May 2021; Accepted: 17 December 2021.

Significance Statement

Metabolic diseases are associated with alteration of neurogenic niche and impairment of cognitive function. Authors demonstrate that insulin resistance alters proliferation of neural stem cells through the inhibition of Forkhead box O transcription factors and the induction of p21-mediated senescence. In physiological conditions, neural stem cells secrete exosomes, which are extracellular vesicles involved in intercellular communication. The intranasal administration of neural stem cell-derived exosomes counteracts the impairment of adult neurogenesis. These findings highlight the potential role of extracellular vesicles to prevent both physiological and pathological cognitive decline.

Introduction

Brain ageing is characterized by impairment of cognitive functions and increased risk of neurodegeneration.[1] Several hallmarks of brain ageing have been described including alteration of synaptic transmission and plasticity, reduction of adult neurogenesis, neuroinflammation, and epigenetic changes.[2] Depletion of the neural stem and progenitor cells (NSPCs) in the adult hippocampal neurogenic niche has been associated with the age-dependent learning and memory deficits in both rodents and humans[3-5] and it could contribute to both physiological and disease-related decline of cognitive functions.[6,7] Among numerous environmental stimuli influencing NSPC proliferation and self-renewal in vivo, nutrient availability, and nutrient-sensing pathways have been demonstrated to play a relevant role in the regulation of NSPC pool maintenance and function.[8,9] In particular, inhibition of the downstream effectors of insulin pathway (ie, Forkhead box O (FoxO) transcription factors) caused premature exhaustion of the NSPC pool.[10] Accordingly, alteration of learning and memory has been observed in both experimental models of insulin resistance and patients with diabetes.[11,12] However, a causal link among reduced adult neurogenesis, accelerated brain ageing, and impairment of cognitive function in diabetes has not been established yet. Adult NSPCs release soluble factors contributing to intercellular communication inside the central nervous system and potentially counteracting the senescence of brain cells.[13-15] We recently demonstrated that NSPC-derived exosomes (exo-NSPC) rescued BDNF-TrkB signaling in the hippocampus and reverted memory deficits in a mouse model of brain insulin resistance (BIR).[16] Therefore, we investigated whether exo-NSPC also affected NSPC pool and adult hippocampal neurogenesis in a well-established mouse model of BIR-dependent cognitive impairment, such as mice fed a high-fat diet (HFD).[17] Here, we demonstrated that HFD reduced NSPC proliferation and promoted senescence of self-renewing cells. Insulin resistance caused inactivation of both FoxO1 and FoxO3a transcription factors leading to inhibition of genes controlling proliferation and stemness, and enhancement of senescence marker p21Waf1/Cip1/Sdi1 (p21) expression. Finally, intranasal administration of exo-NSPC restored NSPC proliferation and counteracted their senescence in HFD mice thus leading to enhanced adult hippocampal neurogenesis.

Materials and Methods

Ethics and Animal Use Statement

Thirty- to 35-day old C57BL/6 mice derived from the Animal Facility of Università Cattolica del Sacro Cuore (UCSC) were randomly assigned to 2 feeding regimens: (1) standard diet (SD, control) or (2) HFD. Mice were always housed in groups (3-5 animals per cage) and daily monitored. All animal procedures were reviewed and approved on 16/01/2017 by the Ethics Committee of UCSC and were fully compliant with Italian (Ministry of Health guidelines, Legislative Decree No. 116/1992) and European Union (Directive No. 86/609/EEC) legislations on animal research. Methods were carried out in strict accordance with the approved guidelines. The animals were housed under a 12-hour light-dark cycle at room temperature (19–22 °C), fed with their respective diet and water ad libitum and body weight was weekly monitored.

Animals and Treatments

Mice from the same litter have been assigned to different experimental groups. Animals were fed with SD (18.5% proteins; 46% carbohydrates, namely 42% starch, 4% sucrose; 3% fats; 6.55% fat caloric content; cat. num. 4RF21) or HFD (23% proteins; 42% carbohydrates, namely 28% starch, 9% sucrose, 5% maltodextrin; 34% fats; 60% fat caloric content; cat. num. PF4051/D) for 6 weeks. The diets were from Mucedola (Guidonia Montecelio, RM, Italy). For in vivo administration of exo-NSPC, mice were intranasally treated with phosphate-buffered saline (PBS; vehicle) or exo-NSPC (1.5 µg per nostril, 3 times per week) for the entire duration of the diet. To study the NSPC proliferation in vivo, bromodeoxyuridine (BrdU; Sigma; 100 mg/kg dissolved in 0.9% NaCl solution) was intraperitoneally injected for the last 5 days of the dietary regimen.

Cell Cultures and Treatments

Postnatal hippocampal NSPCs were isolated and cultured according to previously published protocols.[18] Briefly, brains of newborn (0-1 days) C57bl/6 mice were microdissected and the hippocampus was isolated upon sagittal sectioning. Tissues were finely minced and digested by accutase (in DPBS, 0.5 mM EDTA; Innovative Cell Tecnologies, Inc., San Diego, CA, USA) at 37 °C for 30 minutes. After centrifugation, cells were dissociated and resuspended in Neurobasal-A medium supplemented with 2% B27 without vitamin A (Gibco), Glutamax (0.5 mM), recombinant mouse Fibroblast Growth Factor basic (10 ng/mL), recombinant human epidermal growth factor (10 ng/mL), and recombinant mouse platelet-derived growth factor-bb (10 ng/mL) (all reagents from Thermo Fisher Scientific, Waltham, MA, USA). Cells were seeded and incubated at 37 °C in a 5% CO^2 atmosphere. After the first week of culture NSPCs began to form neurospheres. At 2-day intervals, the neurospheres were collected and passaged by gentle enzymatic and mechanical dissociation. To obtain monolayer cultures, neurospheres were plated as single cells onto Matrigel Matrix (Becton Dickinson, Franklin Lakes, NJ) precoated Petri dishes.

For extracellular vesicle separation, NSPC medium containing vesicles was collected after the first 1-2 passages of expansion, separated via centrifugation (800*g* 10 minutes), filtered with 0.45 µM filters and frozen at −80 °C until use.

For in vitro experiments, undifferentiated NSPCs obtained by neurosphere dissociation were plated onto coverslips and let to proliferate for 24 hours. After, we treated cells with a cocktail of 20 nM insulin and 0.1 mM palmitic acid (IPA) and 2.5 µg of vesicles/1 × 10^6 cells for 3 days. On the third day 2.5 µM BrdU was added to the NSPC culture medium for 3 hours before fixation.

For the differentiation protocol, NSPCs were cultured in a medium defined as "differentiation medium", in which growth factors were replaced with 1% fetal bovine serum to induce differentiation. Insulin and 0.1 mM palmitic acid was added at the beginning of differentiation and both differentiation medium and IPA were replaced every 2 days. Differentiating NSPCs were cultured up to 6 days.

SH-SY5Y cells were cultured in DMEM/F-12 medium (Sigma-Aldrich). Thirty-six hours after plating, DMEM/F-12 medium was replaced with fresh NSPC medium. After 24 hours, media were collected for extracellular vesicle separation.

Western Blotting

Neural stem and progenitor cells were lysed in ice-cold lysis buffer (NaCl 150 mM, Tris-HCl 50 mM, pH 8, EDTA 2 mM) containing 1% Triton X-100, 0.1% SDS, 1× protease inhibitor cocktail, 1 mM sodium orthovanadate, 1 mM sodium fluoride, and 1mM phenylmethylsulfonyl fluoride (all reagents from Sigma-Aldrich, St. Louis, MO, USA). The lysate was sonicated for 5 minutes using a Diagenode Bioruptor Standard Waterbath Sonicator. Samples were spun down at 13 000*g* at 4 °C for 15 minutes. Supernatant was quantified for protein content using the Bradford method (DC Protein Assay; Bio-Rad, Hercules, CA, USA). Equal amounts of proteins were diluted in Laemmli buffer, boiled and resolved using SDS-PAGE. The primary antibodies (Table S1) were incubated overnight and signals were revealed with HRP-conjugated secondary antibodies (Cell Signaling Technology Inc., Danvers, MA, USA) and chemiluminescent substrates (Cyanagen, Bologna, BO, Italy). Antibody against phospho-TrkB Tyr816 was a kind gift of Moses V. Chao. UVItec Cambridge Alliance was used to detect and quantify the signal. Expression levels of the target protein were normalized on the housekeeping protein ACTIN in each lane. Phosphorylation levels of the target protein were normalized on the total amount of the target protein in each lane. In each bar graph, the mean value of controls was set to 1 and the expression or phosphorylation levels of the target protein were shown as fold changes compared with the control (relative units). Representative images of Western blots were only cropped for presentation with no manipulations.

RNA Analyses

Total RNA was extracted using an RNAqueous Micro Kit (Ambion Inc., Austin, TX, USA) according to the manufacturer's instructions. Equal amounts of RNA (2 µg) were subsequently reverse-transcribed using a high-capacity cDNA reverse transcription kit (Applied Biosystems, Foster City, CA, USA). Quantitative RT-PCR was performed in triplicates using inventoried TaqMan Gene expression assays purchased from Applied Biosystems (probes are shown in Table S2). Relative mRNA levels for genes of interest were normalized to TATA-box-binding protein (TBP), glyceraldehyde 3-phosphate dehydrogenase and hypoxanthine phosphoribosyltransferase 1 (Hprt) taken as housekeeping genes, and calculated by using the $2^{-\Delta\Delta Ct}$ method. Three independent experiments were performed with the ABI 7500 Sequence Detection System Analyzer for RT-qPCR (Applied Biosystems). Results were expressed as mean fold changes induced by IPA treatment compared with control samples.

Chromatin Immunoprecipitation

Neural stem and progenitor cell pellets and dentate gyri isolated from brain slices containing hippocampus were homogenized in lysis buffer containing 1% SDS, 50 mM Tris-HCl (pH 8.0), and 10 mM EDTA and sonicated on ice with 6 10-s pulses with a 20-s interpulse interval. Sample debris was removed via centrifugation, and supernatants were immunoprocessed with 2 µg of anti-FoxO1, anti-FoxO3a, anti-histone H3 lysine 9 acetylation (H3K9ac), or control IgG overnight at 4 °C. Immunocomplexes were collected via incubation with protein-G Sepharose 4B beads (Sigma-Aldrich, St. Louis, MO, USA) for 2 hours at 4 °C. After 7 sequential washes, immunocomplexes were eluted from beads by vortexing in elution buffer (1% SDS and $NaHCO_3$ 0.1 M; pH 8.0). NaCl was added (final concentration 0.33 M), and cross-linking was reversed by incubation overnight at 65 °C. DNA fragments were purified using a PCR DNA fragments purification kit (Geneaid Biotech Ltd., New Taipei City, Taiwan). The antibodies and primer sequences are shown in Supplementary Tables S1 and S3, respectively.

PCR reaction was performed in triplicate. Data are expressed as percentage of input calculated by the "adjusted input value" method according to the manufacturer's instructions (ThermoFisher Scientific ChIP Analysis, Carlsbad, CA, USA).

Immunofluorescence Experiments

Cultured NSPCs were washed in PBS 1× to remove culture medium and fixed with 4% PFA for 15 minutes at room temperature (RT). For BrdU immunostaining, cells were incubated with 2N HCl for 30 minutes at RT. Cells were then permeabilized with 0,2% Triton X-100 in 1× PBS for 10 minutes and blocked with 5% normal goat serum (NGS) in 1× PBS. Incubation with primary antibody (Sox2, Nestin, BrdU, p21, MAP2, GFAP, or p16, 1:200; Table S1) was performed overnight at 4 °C in a humidified chamber. Secondary antibody (Alexa Fluor-488 or -546, 1:500, Invitrogen, Carlsbad, CA, USA) was incubated for 1.5 hours at RT. Nuclei were stained with 4′,6-diamidino-2-phenylindole (DAPI, Invitrogen) for 10 minutes at RT. Cells were mounted on a microscope slide using the mounting medium ProLong Gold antifade reagent (Invitrogen).

For immunohistochemistry experiments and detection of labeled exosomes in vivo, animals were deeply anesthetized and were transcardially perfused with PBS (0.1 M, pH 7.4) followed by 4% PFA. Brains were collected, post-fixed overnight at 4 °C in PFA, and then transferred to a solution of 30% sucrose in 0.1 M PBS. Sagittal or coronal brain sections (40-µm-thick) were cut with vibratome (VT1000S, Leica Microsystems, GmbH, Wetzlar, Germany).

For BrdU/DCX double labeling, sections were processed as previously described.[19] Only for Nestin immunolabeling, an antigen retrieval step (with 10 mM sodium citrate, pH 6.0, and 0.05% Tween 20 at 60 °C in a water bath, overnight) was performed. For Nestin/p21/MAP2 immunohistochemistry, after permeabilization and 1 hour blocking incubation in 1× PBS with 0.3% Triton X-100 (Sigma, St. Louis, MO, USA)

and 5% NGS, tissues were incubated overnight at 4 °C with MAP2 antibody (1:400), p21 (1:200, Abcam), or Nestin (1:200). The next day, tissues were incubated for 90 minutes at RT with the secondary antibody: Alexa Fluor-488 or -546 anti-mouse/rabbit (1:500; Invitrogen). Finally, nuclei were counterstained with DAPI (0.5 µg/mL for 10 minutes; Invitrogen), and slices were coverslipped with ProLong Gold anti-fade reagent.

For the MitoTracker Orange CMTMRos (catalog number: M7510) Vitality assay, which stains mitochondria in living cells, cultured cells were treated with 200 nM MitoTracker Dye for 10 minutes at 37 °C. Cells were then fixed with 4% paraformaldehyde (PFA) and nuclei were labeled with 4′6-diamidino-2- phenylindole (10 minutes at RT). Changes in MitoTracker -related fluorescence intensity (fluorescence intensity signal) were evaluated using the NIS-Elements AR software (fluorescence intensity/area) for each field (n = 4 field for each sample, n = 4 independent samples).

Confocal Image Analysis

Images (1024 × 1024 pixels) were acquired at 20×, 40× or 60× magnification with a Nikon A1 MP confocal system (Tokyo, Japan) and an oil-immersion objective (NA 1.2). For some images, additional magnification was applied and the scale bar was shown in the picture.

For in vitro analyses of BrdU$^+$, p21$^+$, or p16INK4A$^+$ cells, the percentages of immunoreactive cells compared with the total number of DAPI$^+$ cells were calculated in each field. Control values were set to 1 and all other values were indicated as fold changes compared with control (relative units).

For the analysis of differentiated cells (astroglial or neuronal), GFAP$^+$ or MAP2$^+$ cells were counted and compared with the total number of DAPI$^+$ ones. Control values were reported as 1 and all other values were indicated as fold changes compared to control.

To evaluate the immunostaining of p21$^+$ and p16INK4A$^+$ cells, each cell was analyzed as follows. Briefly, the operator drew an ROI around each p21/ p16INK4A-expressing cell and measured fluorescence brightness values through the ImageJ software (RGB pixels are converted to brightness values using the formula V = (R + G + B/3). Since these proteins are normally expressed in physiological conditions, threshold was set at the mean fluorescence value observed in vehicle-treated cells, and p21$^+$ and p16INK4A$^+$ cells exhibiting fluorescence values higher than the threshold were counted.

For in vitro experiments, approximately 1000 cells for each experiment were counted. n values indicate the number of independent experiments (derived from at least 3 different NSPC primary cultures).

For *in vivo* immunofluorescence analyses, DAPI$^+$/BrdU$^+$, DCX$^+$/BrdU$^+$ and Nestin$^+$/BrdU$^+$ cells were counted. For in vivo analysis of Nestin immunolabeling, cells bodies showing an immunoreactivity for Nestin were counted.

For the count of p21$^+$ NSPCs in vivo, we identified proliferating NSPCs of the SGZ of the dentate gyrus of the hippocampus through BrdU incorporation. Using the software NIS Elements AR 5.30.01 and focusing on BrdU$^+$ cells we performed a stack-by-stack analysis which allowed us to evaluate the fluorescence intensity of p21 cell-by-cell along the 3 cross-sections XY, XZ, and YZ (see Fig. S3B). To assess the amount of p21$^+$ cells, both in vivo and in vitro, a threshold in fluorescence intensity was preset by the operator to distinguish between p21$^+$ and p21$^-$ cells. For in vivo experiments at least 6 hippocampal slices from each mouse brain were processed. n values indicate the number of studied mice.

Extracellular Vesicles

Media were collected 24 hours after the last change and frozen at −80 °C. Exosomes were isolated from culture medium using exoEasy Maxi Kit (Qiagen) and multistep centrifugations according to the manufacturer's instructions. The exosomes were quantified with the Bradford method.

The dimensional characterization of exosomes was evaluated by dynamic light scattering (Zetasizer Nano ZS, Malvern, Worcestershire, UK). Data for each sample were collected on a continuous basis for 12 minutes in sets of 4 measurements for each sample.

For analysis with transmission electron microscopy, exosomal samples were fixed with formaldehyde and 2.5% glutaraldehyde in 0.1 mol/L sodium cacodylate buffer (pH 7.4), placed on Formvar-carbon-coated grids and air-dried for 10 minutes. After being rinsed, the exosomes were postfixed in 1.5% osmium tetroxide in 0.1 mol/L cacodylate buffer (pH 7.3) and then allowed to dry. Vesicles were observed with a Zeiss Libra 120 (Zeiss NTSGmbH, Oberkochen, Germany).

For visualization of exosomes in vivo, vesicles were labeled with the fluorescent membrane dye kit ExoGlowTM (ExoGlowTM Membrane EV Labeling Kit, System Biosciences, Palo Alto, CA, USA), following the manufacturer's instructions. Exosomes were incubated with a mixture of reaction buffer and labeling dye for 30 minutes at RT. Labeled exosomes were then separated from unbound fluorescent dye through PD-Spintrap G-25 (GE Healthcare, Chicago, IL, USA). For in vivo localization of exo-NSPC, mice were intranasally treated 3 times (8 µg per nostril). Six hours after the last administration the animals were deeply anesthetized, transcardially perfused, and sacrificed. Brain tissues were handled as described in the Immunofluorescence paragraph.

Statistical Analysis

Sample sizes were chosen with adequate power (0.8) according to results of prior pilot data sets or studies, including our own, which used similar methods or paradigms. Sample estimation and statistical analyses were performed using SigmaPlot 14 software. Data were first tested for equal variance and normality (Shapiro-Wilk test) and the appropriate statistical tests were chosen. The statistical tests used (ie, Student's t test, 2-way ANOVA) are indicated in the main text and in the corresponding figure legends for each experiment. N numbers are reported in the figure legends. Degrees of freedom are n – 1 for each condition in both the unpaired t-test and ANOVA tests. F-values and F critical values are indicated in the text for all ANOVA tests. Post hoc multiple comparisons were performed with Bonferroni correction. All statistical tests were 2-tailed and the level of significance was set at .05. Results are shown as mean ± SEM.

Results

Insulin Resistance Inhibits Proliferation of NSPCs In Vitro

Type 2 diabetes (T2D)-related cognitive impairment is correlated with decreased adult neurogenesis in the hippocampus due to defective proliferation, differentiation, and cell

survival.[20] Adult neurogenesis deficits have also been reported in experimental models of insulin resistance, such as the db/db mice[21] and the Goto-Kakizaki rats.[22] Here we investigated the effects of insulin resistance on intracellular pathways affecting proliferation and senescence of hippocampal NSPCs isolated from newborn wild-type mice. First, we characterized our cellular model by immunoreactivity for markers of stemness as the type VI intermediate filament protein Nestin and the transcriptional factor Sox2 (Fig. 1A), along with investigating NSPC ability to form neurospheres. When exposed to a differentiation protocol NSPSs acquired either neuronal or glial phenotype (a representative image of neuronal and astroglial cells after 6 days of differentiation is shown in Supplementary Fig. S1A). Undifferentiated NSPCs were cultured for 72 hours with a cocktail of insulin and palmitic acid to induce an insulin resistant phenotype as previously demonstrated.[23] Neural stem and progenitor cel;s expressed the insulin receptor β (Supplementary Fig. S1B) and showed hallmarks of insulin resistance upon treatment with IPA. In particular, immunoblot analyses revealed high levels of inhibitory insulin receptor substrate 1 (IRS-1) phosphorylation on serine 612 (+77% of controls, $P = .03$; $n = 5$; Fig. 1B).

To investigate the effects of IPA on NSPC proliferation, we performed BrdU labeling and neurosphere assays (NSA). Insulin resistant NSPCs showed lower number of BrdU-incorporating cells compared with control cells (–39%, $P = .004$; $n = 4$; Fig. 1C). Moreover, we found a significant reduction in the diameter of neurospheres (–45.2%, $P = 1.67 \times 10^{-13}$; $n = 15$; Fig. 1D) with no changes in their number ($P = .22$; $n = 22$; Fig. 1D).

The lower proliferation of IPA-treated NSPCs was associated with a small reduction of cell viability (–12%, $P = .029$; $n = 8$; Supplementary Fig. S1C), assessed by Mitotracker accumulation. More importantly, the expression of genes regulating NSPC proliferation and self-renewal was significantly decreased upon IPA treatment. In IPA-treated NSPCs, a significant reduction of mRNA levels was observed for Cyclin D1, Sox2, Tlx, Id3, Hes1, and Mash1 (–32%, -56%, –28%, –42%, –23%, –13%, respectively; $P < .01$ for all genes; $n = 6$; Fig. 1E). No changes were detected in the expression of Rest and EGFr genes (Fig. 1E) as well as in Neuro D1, Neuro D2 and Neurogenin 1 genes promoting neuronal differentiation of NSPCs (Fig. S1D). Accordingly, the percentage of differentiated cells and the relative distribution of neuronal versus astroglial phenotypes after 6 days of differentiation were not significantly affected by IPA treatment (Supplementary Fig. S1E).

IPA Triggers NSPC Senescence In Vitro

Senescence is a form of adaptive cellular response to different types of stress.[2,24] To investigate whether accelerated senescence contributed to IPA-induced impairment of NSPC proliferation, we evaluated the expression of cyclin-dependent kinase inhibitor 1 (p21) by both Western blotting and immunofluorescence. In the nucleus, p21 mediates cell cycle arrest by triggering a senescence program via p53-dependent and -independent pathways.[25,26] Immunocytochemical experiments showed a significant increase of p21 protein in the nuclei of IPA-treated cells (+70% of controls, $P = .0009$; $n = 4$; Figs. 2A and Supplementary Fig. S2A). Accordingly, immunoblot analysis revealed raised levels of p21 in IPA-treated NSPCs compared with controls (+180%, $P = .039$; VEH $n = 4$, IPA $n = 5$; Fig. 2B). Immunofluorescence experiments also revealed a higher number of NSPCs immunoreactive for p16INK4A upon IPA stimulation (+128% of controls, $P = .012$; $n = 8$; Supplementary Fig. S2B). Taken together, these data demonstrated that IPA-induced insulin resistance caused a premature activation of a senescence program in NSPCs.

IPA Inhibits Both FoxO1 and FoxO3a Transcriptional Activity In Vitro

To identify the molecular mechanism underlying the effects of insulin resistance on NSPC fate, we analyzed the expression and the activation levels of nutrient sensors Sirtuin 1 and 2, cAMP response element-binding protein (CREB) and Forkhead box 'Other' (FoxOs) 1 and 3a, which have been clearly demonstrated to be involved in the metabolic regulation of NSPC proliferation.[9,10]

Immunoblot experiments revealed higher levels of both FoxO1 serine 256 and FoxO3a serine 253 inhibitory phosphorylations in IPA-treated NSPCs compared with controls (pFoxO1/FoxO1 + 90%, $P = .003$; pFoxO3a/Foxo3a +88%, $P = .008$; $n = 4$; $n = 7$; Fig. 3A). Instead, no changes were detected in Sirt1 and Sirt2 expression or CREB activation (Sirt1 $P = .099$; $n = 3$; Sirt2 $P = .605$; $n = 3$; pCreb $P = .801$; $n = 4$; Fig. 3A).

Next, we investigated whether IPA affected the recruitment of FoxO transcription factors on the promoters of genes regulating NSPC proliferation and senescence. Bioinformatic analysis of mouse p21, SOX2, Hes1, and Cyclin D1 loci revealed the presence of several putative FoxO responsive elements (pFRE) on the relative regulatory sequences. Chromatin immunoprecipitation experiments confirmed that FoxO3a and FoxO1 bound Cyclin D1 P1, p21 P2, and SOX2 regulatory sequences and that their binding was significantly decreased by IPA treatment (Cyclin D1 P1: FoxO3a –61.5% $P = 5.69 \times 10^{-5}$, FoxO1 –88.1% $P = 7.99 \times 10^{-8}$; p21 P2: FoxO3a –89.9% $P = 5.87 \times 10^{-12}$, FoxO1 –60.7% $P = 2.67 \times 10^{-7}$; SOX2: FoxO3a –78.3% $P = 4.82 \times 10^{-11}$; $n = 6$; Fig. 3B). Accordingly, the transcriptional activation marker lysine 9 histone 3 acetylation (H3K9ac) was lower on these promoters. In particular, H3K9ac was significantly decreased on CyclinD1 and SOX2 loci (CyclinD1: –52.9% $P = 7.09 \times 10^{-5}$; SOX2: –71.4% $P = 1.004 \times 10^{-8}$; $n = 6$; Fig. 3B), whereas it was enhanced on p21 promoter in IPA-treated NSPCs compared with the controls (+153.3% $P = 8.3 \times 10^{-6}$; $n = 6$; Fig. 3B).

Collectively, these data suggest that IPA-induced alterations of NSPC proliferation and senescence rely on aberrant recruitment of FoxOs proteins on regulatory sequences of key genes as SOX2, CyclinD1, and p21.

NSPC-Derived Exosomes Rescue Proliferation/Senescence Balance of NSPCs In Vitro

We recently reported the ability of exosomal vesicles derived from NSPCs (exo-NSPC) to counteract the detrimental effects of insulin resistance on cognitive function by interfering with the gene expression in differentiated neurons.[16] Therefore, we asked whether exo-NSPC also exerted a beneficial effect on the neurogenic niche by counteracting the IPA-dependent impairment of NSPC proliferation. First, we characterized vesicles purified from NSPC culture media using transmission electron microscopy, dynamic light scattering, and immunoblot analysis (Supplementary Fig. S3A-C). Treatment of cultured

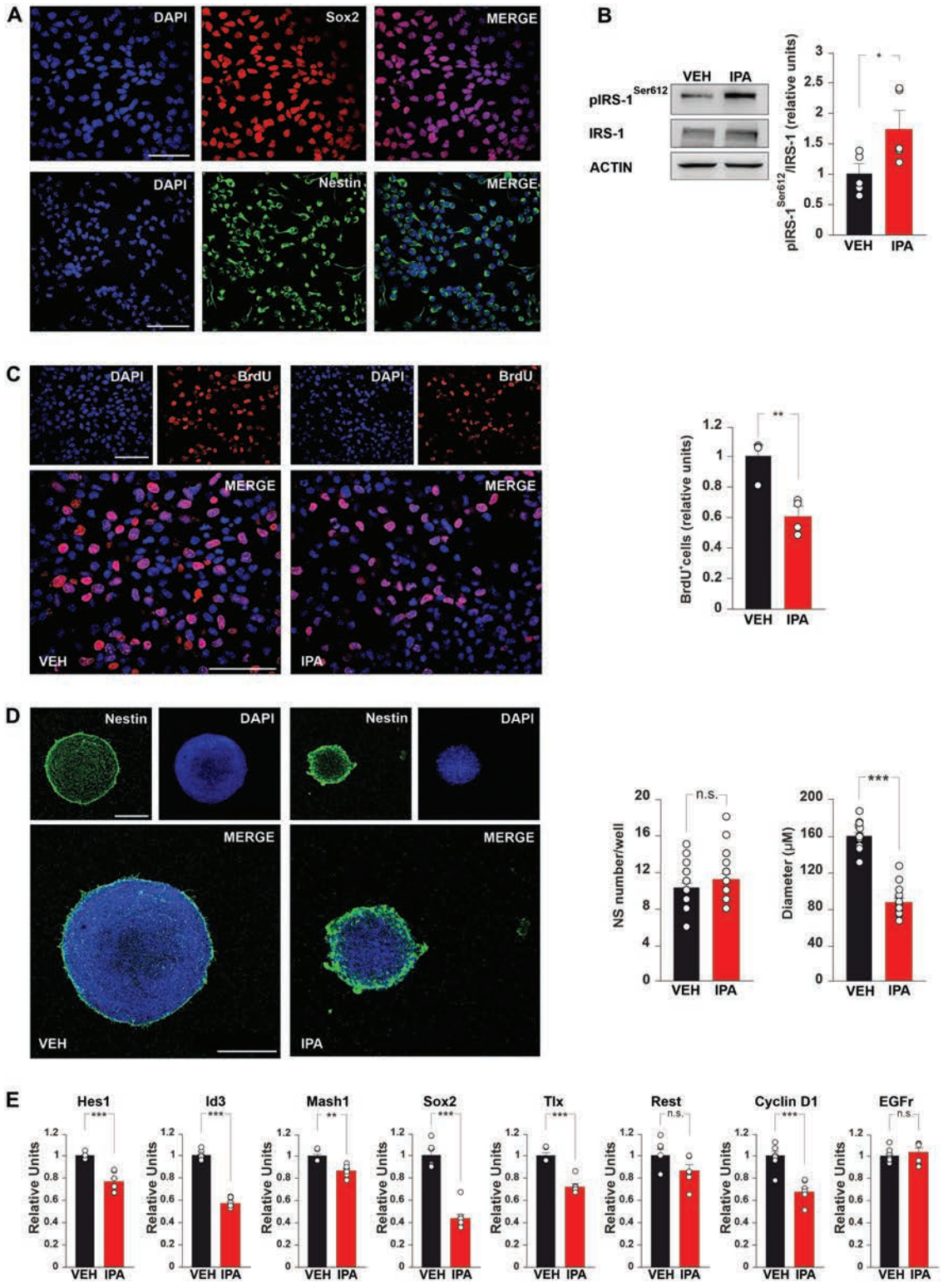

Figure 1. IPA inhibits proliferation of NSPCs in vitro. (**A**) Immunostaining of NSPCs for stemness-related markers Sox2 and Nestin. Scale bar = 50 μm. (**B**) Immunoblots and graph bars showing IRS-1 serine 612 (Ser612) phosphorylation in NSPCs upon stimulation with vehicle (VEH) or insulin and palmitic acid (IPA) ($n = 5$; statistics by unpaired Student's t test). (**C**) BrdU proliferation assay and bar graph showing BrdU immunoreactivity in VEH- and IPA-treated NSPCs ($n = 4$; statistics by unpaired Student's t test). Scale bar = 50 μm. (**D**) Immunostaining of VEH- and IPA-treated neurospheres (NS) for nestin and bar graphs showing number ($n = 22$) and size ($n = 15$) of NS after neurosphere assay (statistics by unpaired Student's t test). Scale bar = 100 μm. (**E**) mRNA expression of different stemness-related genes (Hes1, Id3, Mash1, Sox2, Tlx, Rest, Cyclin D1, and EGFr) in VEH- and IPA-treated NSPCs. ($n = 6$; statistics by unpaired Student's t test). Data are expressed as mean ± SEM. $^{*}P < .05$; $^{**}P < .01$; $^{***}P < .001$; n.s., not significant.

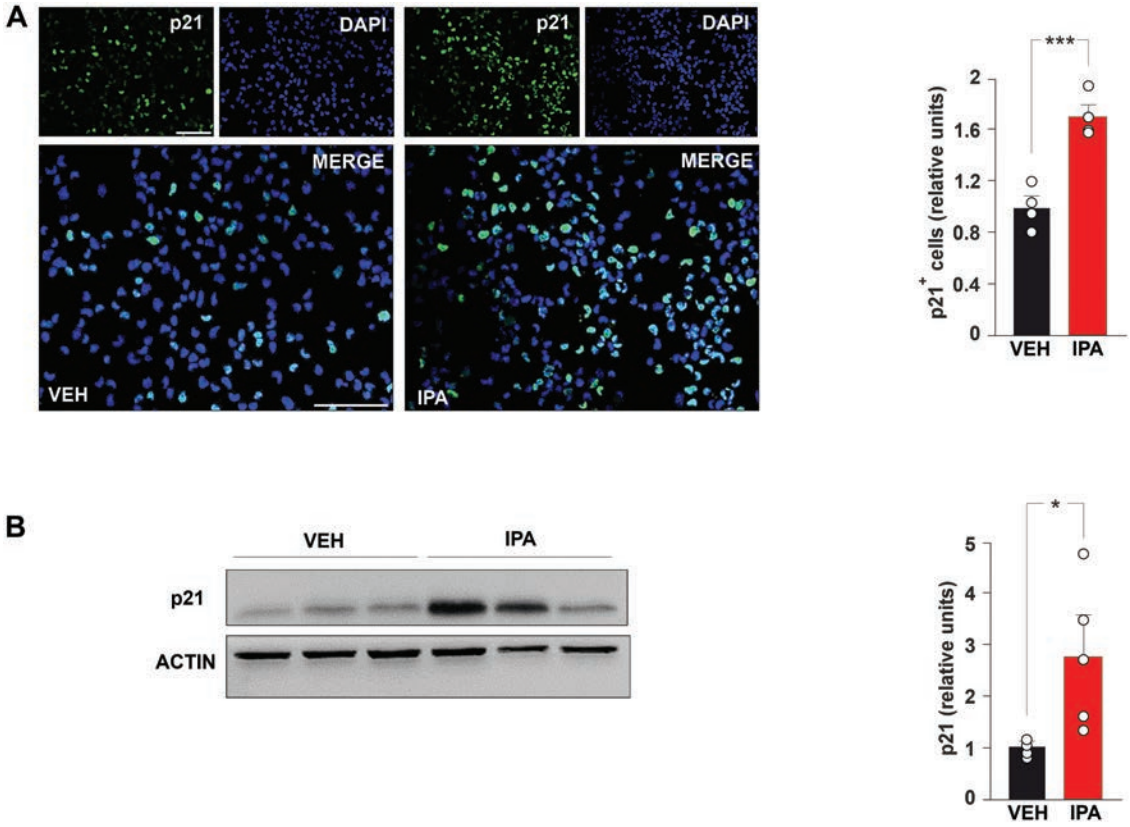

Figure 2. IPA induces premature senescence of NSCs. (**A**) Immunostaining and bar graphs showing the number of p21⁺ cells (see Materials and Methods) in VEH- and IPA-treated cells ($n = 4$; statistics by unpaired Student's t test). (**B**) Immunoblots and bar graphs showing p21 expression in VEH- ($n = 4$) and IPA-treated cells ($n = 5$; statistics by unpaired Student's t test). Scale bar = 50 μm. Data are expressed as mean ± SEM. $*P < .05$; $***P < .001$.

NSPCs with IPA and exo-NSPC for 3 days significantly mitigated IPA-induced downregulation of BrdU-positive cells ($F_{4.10} = 25.52$, IPA vs $IPA_{exo\text{-}NSPC}$ $P = .001$; $n = 6$; Fig. 4A) and produced a remarkable decrease of p21 expression, assessed by both immunofluorescence ($F_{4.45} = 41.04$, IPA vs $IPA_{exo\text{-}NSPC}$ $P = .0005$; $n = 5$; Fig. 4B) and immunoblotting experiments ($F_{5.14} = 9.10$, IPA vs $IPA_{exo\text{-}NSPC}$ $P = .0008$; $n = 4$; Fig. 4C). To investigate the capability of exo-NSPC to also counteract the effects of IPA on both proliferation and senescence of NSPCs, exo-NSPC were administrated for 24 hours after 2 days of IPA treatment ($IPA_{exo\text{-}NSPC\ post}$). Twenty-four hours treatment with exo-NSPC were unable to modify the number of either BrdU⁺ or p21⁺ cells after IPA treatment (BrdU analysis: $F_{3.25} = 7.32$, IPA vs $IPA_{exo\text{-}NSPC\ post}$ $P = .546$; p21 analysis: $F_{3.25} = 7.32$, IPA vs $IPA_{exo\text{-}NSPC\ post}$ $P = .367$; $n = 5$; Supplementary Fig. S3D). To exclude the possibility that the beneficial effects of exo-NSPC depended on any molecules uptaken by vesicles from the culture medium, we performed control experiments in which NSPCs were treated with exosomal vesicles derived from SH-SY5Y cells cultivated with NSPC medium (exo-SH). Of note, exo-SH were not able to counteract the IPA-dependent impairment of both proliferation and senescence of NSPCs (BrdU analysis: $F_{3.25} = 7.32$, IPA vs $IPA_{exo\text{-}SHSY5Y}$ $P = .731$; p21 analysis: $F_{3.25} = 16.36$, IPA vs $IPA_{exo\text{-}SHSY5Y}$ $P = .264$; $n = 5$; Supplementary Fig. S3D).

Our data revealed the capability of exo-NSPC to counteract the IPA-induced alteration of both proliferation and senescence in NSPCs.

Exo-NSPC Reactivate FoxO Transcriptional Activity in Insulin Resistant NSPCs In Vitro

Extracellular vesicles (EVs) contain a plethora of molecules potentially interfering with intracellular molecular cascades.[27] We recently demonstrated that exo-NSPC containing BDNF rescued TrkB activation in the hippocampus of insulin resistant mice.[16] However, in NSPCs the level of TrkB phosphorylation was not significantly changed upon IPA treatment nor following administration of exo-NSPC ($F_{6.94} = 0.504$, $n = 3$; Fig. 5A). Thus, we investigated whether exo-NSPC treatment could modulate the IPA effects on NSPCs by interfering with IRS-1/FoxOs signaling. The analysis of insulin resistance marker IRS-1 Ser612 phosphorylation revealed lower levels in IPA cells upon treatment with exo-NSPC ($F_{4.45} = 9.43$, IPA vs $IPA_{exo\text{-}NSPC}$ $P = .036$; VEH, IPA $n = 5$, $IPA_{exo\text{-}NSPC}$ $n = 6$; Fig. 5B). Moreover, reduced levels of inhibitory FoxO1 and FoxO3a phosphorylation were detected in stem cells upon exo-NSPC treatment, with no significant changes compared to controls (FoxO1: $F_{5.14} = 14.06$, IPA vs $IPA_{exo\text{-}NSPC}$ $P = .007$, VEH vs $IPA_{exo\text{-}NSPC}$ $P = .12$; FoxO3a: $F_{4,45} = 5.21$, IPA vs $IPA_{exo\text{-}NSPC}$ $P = .026$, VEH vs $IPA_{exo\text{-}NSPC}$ $P = .27$; $n = 4$ for FoxO1; $n = 6$ for FoxO3a; Fig. 5B).

Next, we analyzed the effects of exo-NSPC on binding of FoxO transcription factors to the regulatory sequences of Cyclin D1, p21, and SOX2. Both FoxO3a and FoxO1 recruitment on promoters of target genes was increased in IPA-treated cells upon stimulation with exo-NSPC (Cyclin D1 P1: for FoxO3a $F_{4.102} = 17.19$, IPA vs $IPA_{exo\text{-}NSPC}$ $P = .023$,

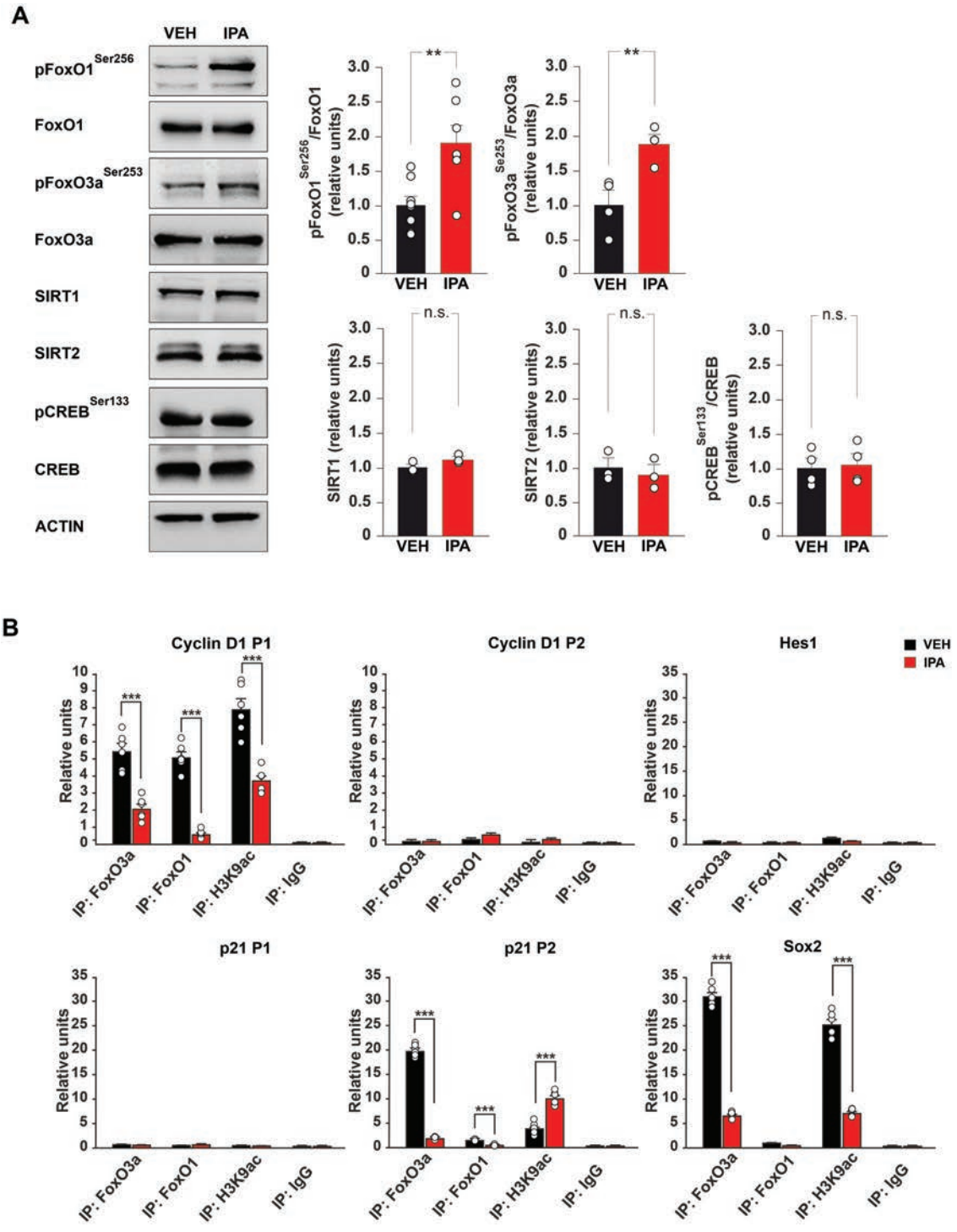

Figure 3. IPA affects the recruitment of both FoxO1 and FoxO3a on the promoters of CyclinD1, p21, and SOX2 genes. (**A**) Immunoblots and bar graphs showing the expression of Sirt1 and Sirt2 ($n = 3$) and the phosphorylation of Creb on serine 133 ($n = 4$), FoxO3a on serine 253 ($n = 4$), and FoxO1 on serine 256 ($n = 7$) in VEH- and IPA-treated cells (statistics by unpaired Student's t test). (B) ChIP assays of FoxO3a, FoxO1, and histone 3 lysine 9 acetylation (H3K9ac) on the promoters of Cyclin D1 (P1 and P2), Hes1, p21 (P1 and P2), and Sox2 genes in VEH- and IPA-treated cells. IgG are used as negative controls. Real-time analysis was performed in triplicate. ($n = 6$; statistics by unpaired Student's t test). Data are expressed as mean ± SEM. $^{**}P < .01$; $^{***}P < .001$; n.s., not significant.

for FoxO1 $F_{4,102} = 78.41$, IPA vs $IPA_{exo\text{-}NSPC}$ $P = 1.96 \times 10^{-5}$; SOX2: for FoxO3a $F_{4,102} = 76.23$, IPA vs $IPA_{exo\text{-}NSPC}$ $P = .002$; p21 P2: for FoxO3a $F_{4,102} = 195.56$, IPA vs $IPA_{exo\text{-}NSPC}$ $P = 1.93 \times 10^{-5}$; $n = 6$; Fig. 5C). Finally, changes of H3K9ac levels on the same loci were almost completely prevented in insulin resistant cells by administration of exo-NSPC (Cyclin D1 P1: $F_{4,102} = 15.21$, IPA vs $IPA_{exo\text{-}NSPC}$ $P = .004$; SOX2: $F_{4,102} = 41.09$, IPA vs $IPA_{exo\text{-}NSPC}$ $P = 1.14 \times 10^{-4}$; p21 P2: $F_{4,102} = 48.43$, IPA vs $IPA_{exo\text{-}NSPC}$ $P = 1.42 \times 10^{-5}$; $n = 6$; Fig. 5C).

Collectively, these data indicated that exo-NSPC affected NSPC fate by modulating the recruitment of FoxO transcription factors on the promoters of genes regulating proliferation and senescence of stem cells.

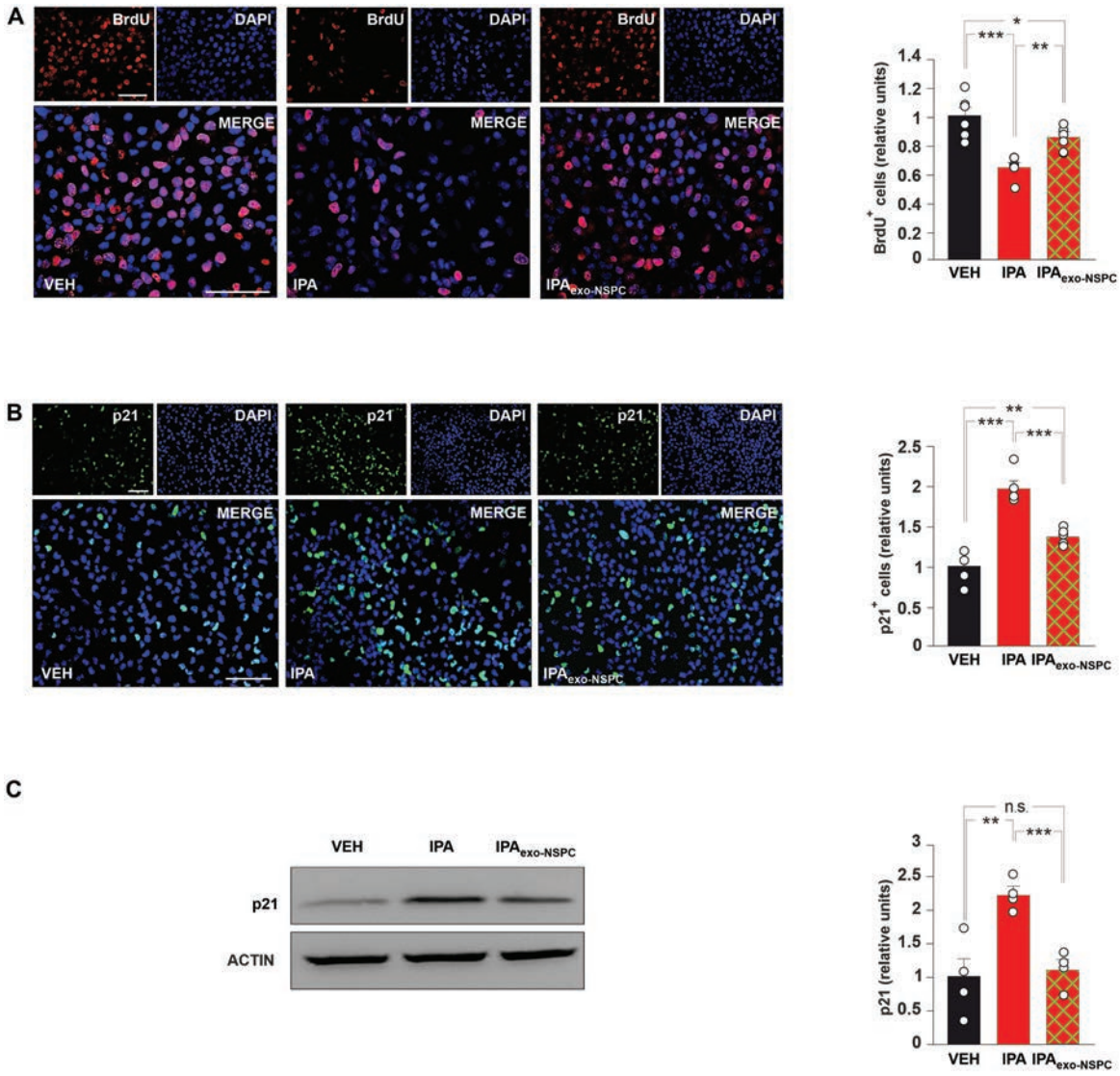

Figure 4. NSPC-derived exosomes counteract IPA-induced alterations of both proliferation and senescence of NSPCs. (A) Representative images and bar graphs of BrdU proliferation assay in NSCs cultivated in either control (VEH) or IPA conditions and treated with vehicle (VEH, IPA) or NSC-derived exosomes ($IPA_{exo\text{-}NSPC}$) ($n = 6$; statistics by 2-way ANOVA and Bonferroni post hoc). Scale bar = 50 μm. (**B**) Immunostaining and bar graphs showing p21 fluorescence intensity signal in VEH-, IPA-, and $IPA_{exo\text{-}NSPC}$-treated cells ($n = 5$; statistics by 2-way ANOVA and Bonferroni post hoc). (**C**) Immunoblots and bar graphs showing p21 expression in VEH, IPA, and $IPA_{exo\text{-}NSPC}$ cells ($n = 4$; statistics by 2-way ANOVA and Bonferroni post hoc). Scale bar = 50 μm. Data are expressed as mean ± SEM. $*P < .05$; $**P < .01$; $*** P < .001$; n.s., not significant.

Exo-NSPC Rescue Adult Hippocampal Neurogenesis in HFD Mice

Next, we asked whether exo-NSPC treatment also modulated adult hippocampal neurogenesis in insulin resistant mice. Exosomes have been implicated in intercellular communications and their cargo can promote the development of neural circuits by acting on neurogenic niches.[28-30] To test the ability of these vesicles to foster and preserve the NSPC niche in the hippocampus of HFD-dependent brain insulin resistant mice, we first documented the capability of intranasal administration to deliver exo-NSPC into the hippocampus of mice (Supplementary Fig. S4A). After, we evaluated the effects of exosomal vesicles on proliferation and stemness in the SGZ of both SD and HFD mice. High-fat diet mice showed lower number of cells immunoreactive for both the stemness-related protein Nestin and the proliferation marker BrdU, and exo-NSPC treatment rescued these alterations (Nestin$^+$ cells: $F_{3.862} = 7.303$, SD_{veh} vs HFD_{veh} $P = .008$, HFD_{veh} vs $HFD_{exo\text{-}NSPC}$ $P = .039$, SD_{veh} vs $HFD_{exo\text{-}NSPC}$ $P = .158$; BrdU$^+$ cells: $F_{3.862} = 20.011$, SD_{veh} vs HFD_{veh} $P = .047$, HFD_{veh} vs $HFD_{exo\text{-}NSPC}$ $P = 4.47 \times 10^{-5}$, SD_{veh} vs $HFD_{exo\text{-}NSPC}$ $P = .02$; $n = 4$ mice; Fig. 6A, C). Similar results were also obtained when we counted the Nestin$^+$/BrdU$^+$ double-labeled cells ($F_{3.49} = 15.477$, SD_{veh} vs HFD_{veh} $P = .0019$, HFD_{veh} vs $HFD_{exo\text{-}NSPC}$ $P = .017$; $n = 5$ mice; Supplementary Fig. S4B). Moreover, exo-NSPC counteracted the increase of senescent p21$^+$ NSPCs induced by HFD in the hippocampus ($F_{3.862} = 13.191$, SD_{veh} vs HFD_{veh} $P = .005$, HFD_{veh} vs $HFD_{exo\text{-}NSPC}$ $P = .013$, SD_{veh} vs $HFD_{exo\text{-}NSPC}$ $P = .222$; $n = 4$ mice; Fig. 6D and Supplementary Fig. S4C).

In HFD mice reduced proliferation and enhanced senescence of NSPCs resulted in decreased hippocampal neurogenesis, assessed by cells double-labeled for BrdU and the marker of immature neurons DCX (BrdU$^+$/DCX$^+$ cells $F_{3.862} = 5.445$, SD_{veh} vs HFD_{veh} $P = .013$; Fig. 6B,E). Of note, the

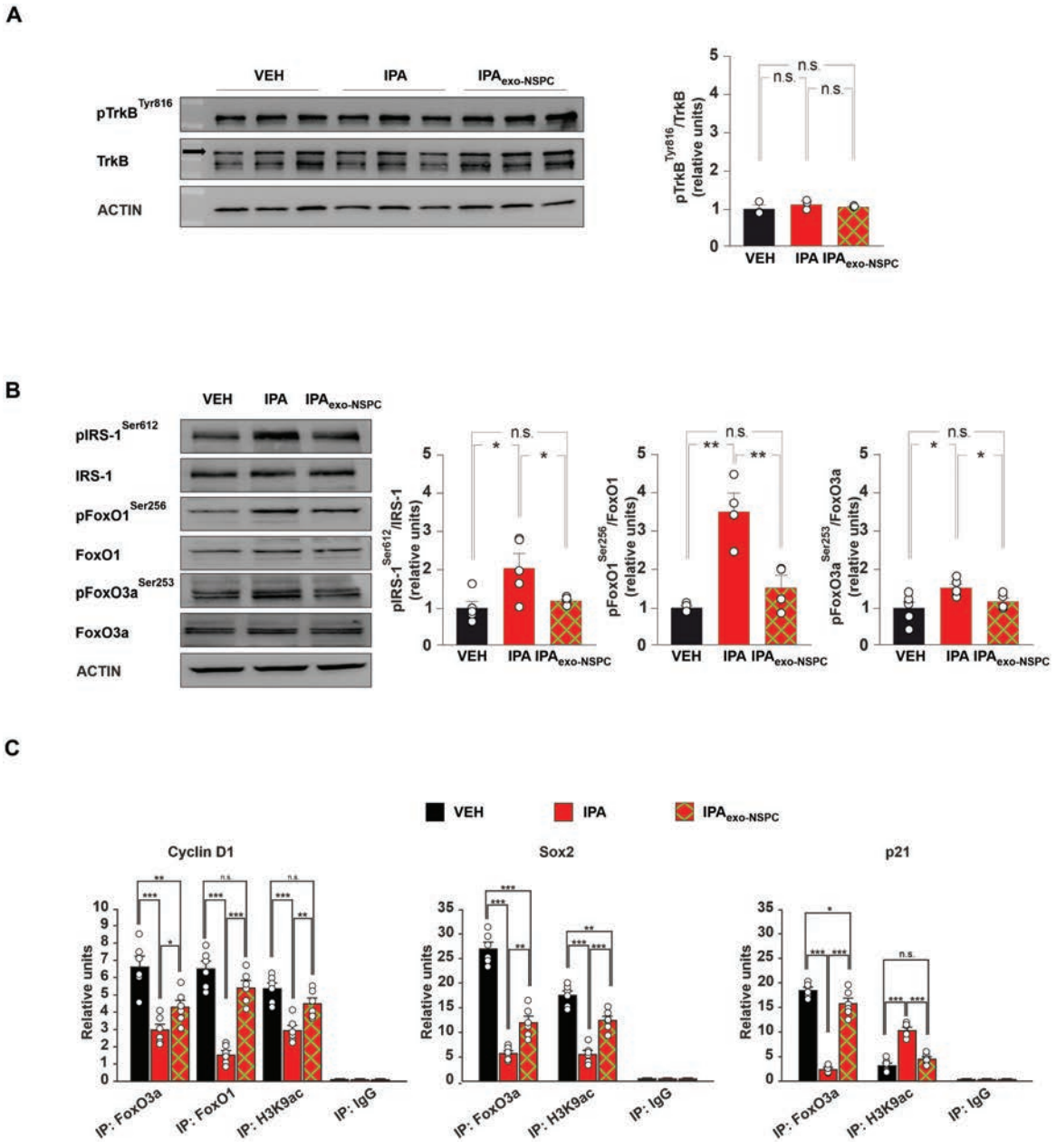

Figure 5. NSPC-derived exosomes restore the transcriptional activity of both FoxO1 and FoxO3a. (**A**) Immunoblots and bar graphs showing phosphorylation levels of TrkB^{Tyr816} (n = 3), in VEH, IPA, and IPA$_{exo\text{-}NSPC}$ cells (statistics by 2-way ANOVA and Bonferroni post hoc). (**B**) Immunoblots and bar graphs showing phosphorylation levels of FoxO1^{Ser356} (n = 4), IRS-1^{Ser612} (n = 5), and FoxO3a^{Ser253} (n = 6) in VEH, IPA, and IPA$_{exo\text{-}NSPC}$ cells (statistics by 2-way ANOVA and Bonferroni post hoc). (C) ChIP assays of FoxO3a, FoxO1, and H3K9ac on the promoters of Cyclin D1 (P1), Sox2, and p21 (P2) genes VEH, IPA, and IPA$_{exo\text{-}NSPC}$ cells. IgG are used as negative controls. Real-time analysis was performed in triplicate (n = 6; statistics by 2-way ANOVA and Bonferroni post hoc). Data are expressed as mean ± SEM. $*P < .05$; $**P < .01$; $*** P < .001$; n.s., not significant.

number of BrdU$^+$/DCX$^+$ cells was fully restored upon treatment with exo-NSPC ($F_{3.862}$ = 5.445, HFD$_{veh}$ vs HFD$_{exo\text{-}NSPC}$ P = .011, SD$_{veh}$ vs HFD$_{exo\text{-}NSPC}$ P = .742; n = 4 mice; Fig. 6B, E). In SD mice, administration of exo-NSPC failed to significantly modify the numbers of either BrdU$^+$ or BrdU$^+$/DCX$^+$ cells.

Finally, ChIP analyses performed on dentate gyrus extracts of mice revealed a decrease of FoxO3 recruitment on the promoters of Cyclin D1, SOX2, and p21 genes and lower levels of H3K9ac on Cyclin D1 and SOX2 promoters in HFD animals. Moreover, exo-NSC administration almost completely re-established the binding of FoxO3a and the epigenetic activation on the same regulatory sequences (Cyclin D1 P1: for FoxO3a $F_{3.287}$ = 24.11, SD$_{veh}$ vs HFD$_{veh}$ $P = 1.92 \times 10^{-5}$, HFD$_{veh}$ vs HFD$_{exo\text{-}NSPC}$ $P = 1.32 \times 10^{-4}$, SD$_{veh}$ vs HFD$_{exo\text{-}NSPC}$ P = .098; for H3K9ac $F_{3.287}$ = 7.702, SD$_{veh}$ vs HFD$_{veh}$ P = .007, HFD$_{veh}$ vs HFD$_{exo\text{-}NSPC}$ $P = 5.67 \times 10^{-4}$, SD$_{veh}$ vs HFD$_{exo\text{-}NSPC}$ P = .549; SOX2: for FoxO3a $F_{3.287}$ = 13.33, SD$_{veh}$ vs HFD$_{veh}$ $P = 3.56 \times 10^{-4}$, HFD$_{veh}$ vs HFD$_{exo\text{-}NSPC}$ $P = 8.94 \times 10^{-6}$, SD$_{veh}$ vs HFD$_{exo\text{-}NSPC}$ P = .301; for H3K9ac $F_{3.287}$ = 17.51, SD$_{veh}$ vs HFD$_{veh}$ $P = 1.54 \times 10^{-5}$, HFD$_{veh}$ vs HFD$_{exo\text{-}NSPC}$ $P = 2.03 \times 10^{-5}$, SD$_{veh}$ vs HFD$_{exo\text{-}NSPC}$ P = .153; p21: for FoxO3a $F_{3.287}$ = 7.187, SD$_{veh}$ vs HFD$_{veh}$ P = .003, HFD$_{veh}$ vs HFD$_{exo\text{-}NSPC}$ P = .002, SD$_{veh}$ vs HFD$_{exo\text{-}NSPC}$ P = .929; n = 6; Fig. 6F).

Collectively, our data showed that exo-NSPC also modulated both proliferation and senescence of NSPCs in vivo,

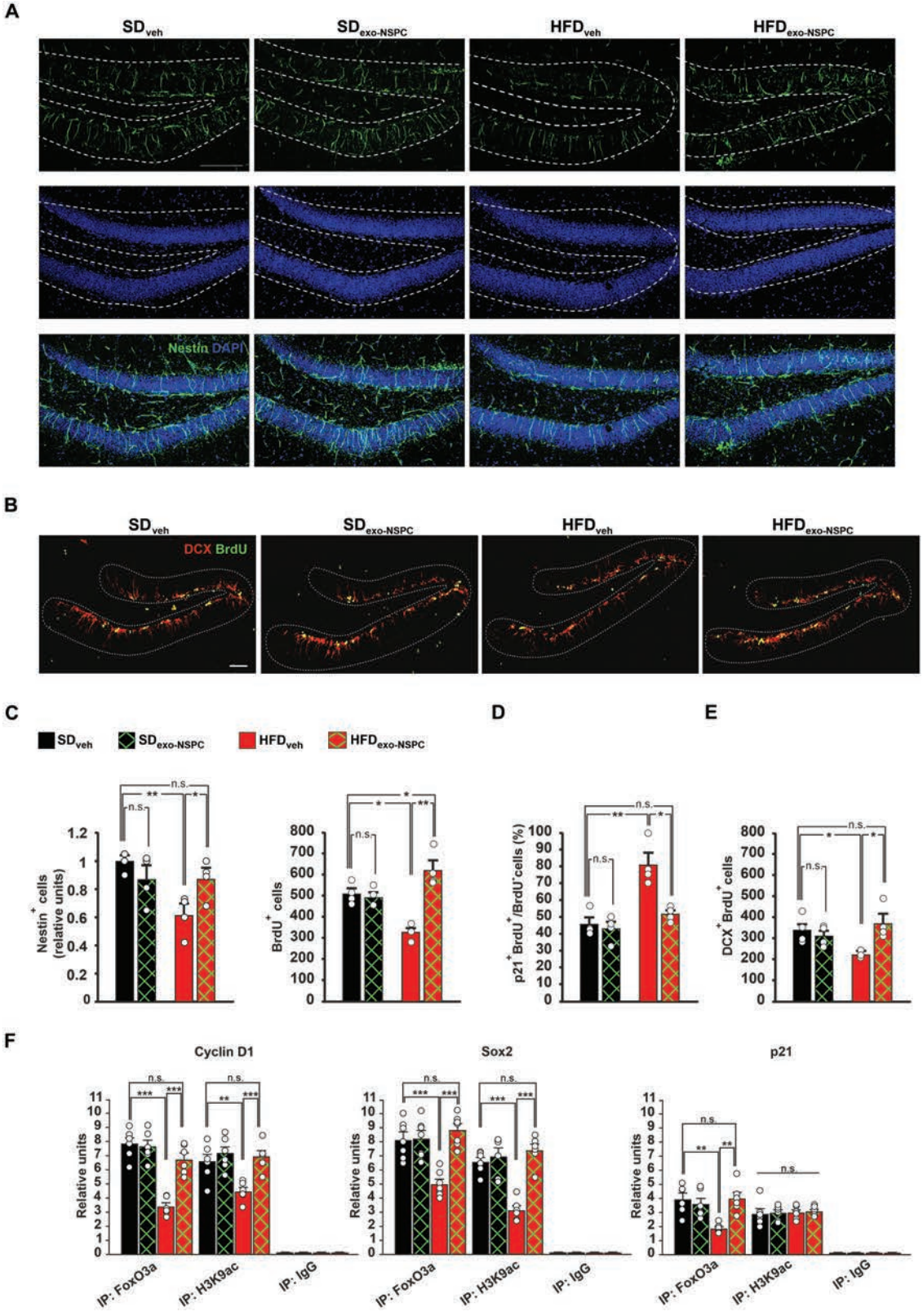

Figure 6. Exo-NSPC counteract HFD-dependent alteration of the neurogenic niche in vivo. (**A**) Immunostaining of Nestin$^+$ cells in hippocampal slices containing subgranular zone (SGZ) of mice fed with SD or HFD and intranasally injected with vehicle (SD_{veh} and HFD_{veh}) or exo-NSPC ($SD_{exo\text{-}NSPC}$ and $HFD_{exo\text{-}NSPC}$) ($n = 4$ mice per group; $n = 7$ slices per animal; statistics by 2-way ANOVA and Bonferroni post hoc). Scale bar = 50 μm. (**B**) Immunostaining of DCX$^+$/BrdU$^+$ cells in hippocampal slices containing SGZ of SD_{veh}, $SD_{exo\text{-}NSPC}$, HFD_{veh}, and $HFD_{exo\text{-}NSPC}$ mice ($n = 4$ per group; $n = 7$ slices per animal; statistics by 2-way ANOVA and Bonferroni post hoc). Scale bar = 50 μm. (**C**) Bar graphs showing the change of Nestin$^+$ cells (left), the number of BrdU$^+$ cells (middle) and the number of DCX$^+$/BrdU$^+$ cells (right) in SD_{veh}, $SD_{exo\text{-}NSPC}$, HFD_{veh}, and $HFD_{exo\text{-}NSPC}$ mice ($n = 4$ per group; $n = 7$ slices per animal; statistics by 2-way ANOVA and Bonferroni post hoc). (D) Bar graphs showing the percentage of BrdU$^+$ cells positive for senescence marker p21 among in SD_{veh}, $SD_{exo\text{-}NSPC}$, HFD_{veh}, and $HFD_{exo\text{-}NSPC}$ mice ($n = 4$ per group; $n = 7$ slices per animal; statistics by 2-way ANOVA and Bonferroni post hoc). Data are expressed as mean ± SEM. $*P < .05$; $**P < .01$; n.s., not significant.

thus counteracting HFD-dependent alterations of the neurogenic niche in the hippocampal SGZ.

Discussion

Brain ageing is a physiological chronic process regulated by intrinsic and external stimuli including metabolic factors, inflammatory molecules, epigenetic changes, and oxygen availability.[2] Alteration of insulin signaling can accelerate brain ageing and cause impairment of cognitive functions.[31] Attention and memory deficits have been reported in patients affected by metabolic disorders such as insulin resistance and T2D.[32,33] The mechanisms contributing to cognitive decline are not fully understood but they may involve a feedback loop of multiple interacting cellular and molecular events including altered nutrient sensing, stem cell exhaustion, mitochondrial dysfunction, alteration of protein homeostasis, glial cell activation, and aberrant intercellular communication, impinging on both NSPCs and differentiated neurons as well as on glial cells.[34] Here, we demonstrated that in vitro overstimulation of insulin signaling in NSPCs induced insulin resistance and inhibited NSPC proliferation (Fig. 1A-D). Moreover, IPA-treated NSPCs showed higher levels of the nuclear senescence markers p21 and p16INK4A (Fig. 2A, B and Supplementary Fig. S2B), which induce cell proliferation arrest. Insulin/IGF-I pathway activation has been reported to promote adult neurogenesis by stimulating NSPC proliferation, differentiation, and survival.[35,36] Conversely, streptozotocin-induced T2D experimental models showed reduced insulin levels and impaired adult hippocampal neurogenesis.[12,22] Nutrient-dependent signals have been clearly demonstrated to impact on brain stem cell niche and to modulate the NSPC fate by interfering with the activity of nutrient sensors regulating chromatin remodeling and gene expression.[37-41] In insulin resistant NSPCs, we found inhibition of both insulin downstream effectors FoxO1 and FoxO3a, which led to reduced recruitment of FoxO transcription factors on the promoters of genes regulating NSPC proliferation (Fig. 3A,B). Conversely, the total number of differentiated cells and the commitment of NSPCs toward neural or glial lineage was not significantly modified upon IPA treatment (Supplementary Fig. S1E). Importantly, the IPA-dependent lower binding of FoxO3a at the promoter of p21 gene resulted in higher levels of transcriptional marker H3K9ac (Fig. 3B). Accordingly the number of $p21^+$ and $p16ink4a^+$ cells was enhanced by IPA treatment (Fig. 2A and Supplementary Fig. S2B). This evidence suggests that the insulin resistance-dependent decrease of NSPC proliferation is independent on accelerated differentiation and it is associated with the increase of stem cell senescence.

Our findings reveal that exo-NSPC rebalanced the recruitment of FoxO transcription factors on the promoters of Cyclin D1, SOX2, and p21 genes (Fig. 5C) and counteracted the effects of IPA on both proliferation and senescence of NSPC in vitro (Fig. 4A-C). Extracellular vesicles may regulate NSPC niche through different mechanisms. It has been demonstrated that EVs transfer between young and senescent cells can induce either a pro-longevity or an SASP phenotype, respectively, via miRNA exchange.[14,42] We recently discovered that exo-NSPC carry neurotrophic factors able to modulate signal transduction and gene expression in neurons.[16] However, the BDNF/TrkB/CREB axis does not appear to play a prominent role in the effects of both insulin resistance and exo-NSPC on NSPCs (Figs. 3A and 5A). Moreover, EVs contain metabolites such as nicotinamide phosphoribosyltransferase that stimulates NAD biosynthesis in the target cells, ameliorates cognitive functions, and extends lifespan in mice.[43] Another intriguing hypothesis is that exo-NSPC cargo may spread several anti-inflammatory mediators that preserve the NSPC reservoir. Further studies are necessary to characterize the exo-NSPC cargo. Perinatal hippocampal neurogenic niche contains a heterogeneous pool of neural stem cell populations that may not perfectly resemble the adult neurogenesis occurring in the SGZ of adult mice. However, in vivo delivery of exo-NSPC to the hippocampus of mice rescued the HFD-dependent impairment of NSPC proliferation in the SGZ of the hippocampal dentate gyrus by preserving the stemness of NSPC pool (Fig. 6A-E). Future studies will clarify whether treatments with EVs can revert an already established damage in addition to antagonize the detrimental effects of HFD on neurogenic niches.

Conclusion

Our findings identified a novel molecular circuit converging on FoxO-mediated transcription of pro-proliferative and pro-senescence genes that underlies the insulin resistance-dependent exhaustion of NSPC pool. The evidence that molecular signals inside the exo-NSPC were sufficient to regulate the NSPC fate opens the way to novel personalized medicine-based studies aimed to investigate the therapeutic potential of these vesicles in both neurological and metabolic disorders. Identifying the senolytic components of exo-NSPC cargo that are able to modulate the adult hippocampal neurogenesis will be a great challenge for the regenerative medicine in the next years.

Acknowledgments

This research was supported by the Italian Ministry of Health (GR-2018-12366381 to S.F.) and intramural grants from the Università Cattolica del Sacro Cuore (Linea D.3.2 2017 to C.G.).

Conflict of Interest

The authors declare no conflict of interest and indicate no financial relationships.

Author Contributions

S.F. and C.G. conceived the study and supervised the work; F.N. performed immunofluorescence and Western blotting experiments; L.L. performed NSC cultures and gene expression analysis; M.R. performed in vivo treatments; S.A.B., R.S., and F.L.G. performed immunohistochemical analyses; M.S. performed exosomes isolation, T.E.M. and D.L.S. analyses; S.F., F.N., and C.G. wrote the paper and all authors commented on the manuscript and approved its final version.

Data Availability

The authors confirm that the data supporting the findings of this study are available within the article and its supplementary materials.

References

1. Kapogiannis D, Mattson MP. Disrupted energy metabolism and neuronal circuit dysfunction in cognitive impairment and Alzheimer's disease. *Lancet Neurol.* 2011;10(2):187-198. https://doi.org/10.1016/S1474-4422(10)70277-5
2. Nicaise AM, Willis CM, Crocker SJ, et al. Stem cells of the aging brain. *Front Aging Neurosci.* 2020;12:247. https://doi.org/10.3389/fnagi.2020.00247
3. Kuhn HG, Dickinson-Anson H, Gage FH. Neurogenesis in the dentate gyrus of the adult rat: age-related decrease of neuronal progenitor proliferation. *J Neurosci.* 1996;16(6):2027-2033. https://doi.org/10.1523/JNEUROSCI.16-06-02027.1996
4. Bondolfi L, Ermini F, Long JM, et al. Impact of age and caloric restriction on neurogenesis in the dentate gyrus of C57BL/6 mice. *Neurobiol Aging.* 2004;25(3):333-340. https://doi.org/10.1016/S0197-4580(03)00083-6
5. Tobin MK, Musaraca K, Disouky A, et al. Human hippocampal neurogenesis persists in aged adults and Alzheimer's disease patients. *Cell Stem Cell.* 2019;24(6):974-982.e3. https://doi.org/10.1016/j.stem.2019.05.003
6. McAvoy KM, Scobie KN, Berger S, et al. Modulating neuronal competition dynamics in the dentate gyrus to rejuvenate aging memory circuits. *Neuron*. 2016; 91(6):1356-1373. https://doi.org/10.1016/jneuron.2016.08.009.
7. Navarro Negredo P, Yeo RW, Brunet A. Aging and rejuvenation of neural stem cells and their niches. *Cell Stem Cell* 2020 Aug 6;27(2):202-223. https://doi.org/10.1016/j.stem.2020.07.002
8. Paik JH, Ding Z, Narurkar R, et al. FoxOs cooperatively regulate diverse pathways governing neural stem cell homeostasis. *Cell Stem Cell* 2009;5(5):540-553. https://doi.org/10.1016/j.stem.2009.09.013
9. Yeo H, Lyssiotis CA, Zhang Y, et al. FoxO3 coordinates metabolic pathways to maintain redox balance in neural stem cells. *EMBO J.* 2013;32(19):2589-2602. https://doi.org/10.1038/emboj.2013.186
10. Renault VM, Rafalski VA, Morgan AA, et al. FoxO3 regulates neural stem cell homeostasis. *Cell Stem Cell* 2009;5(5):527-539. https://doi.org/10.1016/j.stem.2009.09.014
11. Kodl CT, Seaquist ER. Cognitive dysfunction and diabetes mellitus. *Endocr Rev.* 2008 Jun;29(4):494-511. https://doi.org/10.1210/er.2007-0034
12. Mainardi M, Fusco S, Grassi C. Modulation of hippocampal neural plasticity by glucose-related signaling. *Neural Plast.* 2015;2015:657928. https://doi.org/10.1155/2015/657928
13. Cossetti C, Iraci, N, et al. Extracellular vesicles from neural stem cells transfer IFN-γ via Ifngr1 to activate Stat1 signaling in target cells. *Mol Cell.* 2014;56(2):193-204. https://doi.org/10.1016/j.molcel.2014.08.020
14. Zhang Y, Kim MS, Jia B, et al. Hypothalamic stem cells control ageing speed partly through exosomal miRNAs. *Nature. 2017;548(7665):52-57. doi: 10.1038/nature23282. Epub 2017 Jul 26. Erratum in: Nature*. 2018 Aug;560(7719):E33.
15. Vogel A, Upadhya R, Shetty AK. Neural stem cell derived extracellular vesicles: Attributes and prospects for treating neurodegenerative disorders. *EBioMedicine*. 2018 Dec;38:273-282. https://doi.org/10.1016/j.ebiom.2018.11.026
16. Spinelli M, Natale F, Rinaudo M, et al. Neural stem cell-derived exosomes revert HFD-dependent memory impairment via CREB-BDNF signalling. *Int J Mol Sci* . 2020 Nov 26;21(23):8994. https://doi.org/10.3390/ijms21238994
17. Mainardi M, Spinelli M, Scala F, et al. Loss of leptin-induced modulation of hippocampal synaptic trasmission and signal transduction in high-fat diet-fed Mice. *Front Cell Neurosci.* 2017 Jul 28;11:225. https://doi.org/10.3389/fncel.2017.00225
18 Leone L, Colussi C, Gironi K, et al. Altered Nup153 expression impairs the function of cultured hippocampal neural stem cells isolated from a mouse model of Alzheimer's disease. *Mol Neurobiol.* 2019 Aug;56(8):5934-5949. https://doi.org/10.1007/s12035-018-1466-1
19. Fusco S, Leone L, Barbati SA, et al. A CREB-Sirt1-Hes1 circuitry mediates neural stem cell response to glucose availability. *Cell Rep* 2016;14(5):1195-1205. https://doi.org/10.1016/j.celrep.2015.12.092
20. Winner B, Kohl Z, Gage FH. Neurodegenerative disease and adult neurogenesis. *Eur J Neurosci.* 2011 Mar;33(6):1139-1151. https://doi.org/10.1111/j.1460-9568.2011.07613.x
21. Stranahan AM, Arumugam TV, Cutler RG, et al. Diabetes impairs hippocampal function through glucocorticoid-mediated effects on new and mature neurons. *Nat Neurosci.* 2008 Mar;11(3):309-317. https://doi.org/10.1038/nn2055
22. Lang BT, Yan Y, Dempsey RJ, et al. Impaired neurogenesis in adult type-2 diabetic rats. *Brain Res*. 2008;1258:25-33.
23. Spinelli M, Fusco S, Mainardi M, et al Brain insulin resistance impairs hippocampal synaptic plasticity and memory by increasing GluA1 palmitoylation through FoxO3a. *Nat Commun.* 2017 Dec 8;8(1):2009. https://doi.org/10.1038/s41467-017-02221-9
24. Fridlyanskaya I, Alekseenko L, Nikolsky N. Senescence as a general cellular response to stress: a mini-review. *Exp Gerontol.* 2015 Dec;72:124-128. https://doi.org/10.1016/j.exger.2015.09.021
25. Abbas T, Dutta A. p21 in cancer: intricate networks and multiple activities. *Nat Rev Cancer.* 2009;9(6):400-414. https://doi.org/10.1038/nrc2657
26. Romanov VS, Pospelov VA, Pospelova TV. Cyclin-dependent kinase inhibitor p21(Waf1): contemporary view on its role in senescence and oncogenesis. *Biochemistry (Mosc)* 2012;77(6):575-584. https://doi.org/10.1134/S000629791206003X
27. Budnik V, Ruiz-Cañada C, Wendler F. Extracellular vesicles round off communication in the nervous system. *Nat Rev Neurosci.* 2016;17(3):160-172. https://doi.org/10.1038/nrn.2015.29
28. Zhang G, Zhu Z, Wang H, et al. Exosomes derived from human neural stem cells stimulated by interferon gamma improve therapeutic ability in ischemic stroke model. *J Adv Res*. 2020;24:435-445. https://doi.org/10.1016/j.jare.2020.05.017
29. Sharma P, Mesci P, Carromeu C, et al. Exosomes regulate neurogenesis and circuit assembly. *Proc Natl Acad Sci USA*. 2019;116(32):16086-16094. https://doi.org/10.1073/pnas.1902513116
30. Iraci N, Gaude E, Leonardi T, et al. Extracellular vesicles are independent metabolic units with asparaginase activity. *Nat Chem Biol.* 2017;13(9):951-955. https://doi.org/10.1038/nchembio.2422
31. Spinelli M, Fusco S, Grassi C. Brain insulin resistance impairs hippocampal plasticity. *Vitam Horm.* 2020;114:281-306. https://doi.org/10.1016/bs.vh.2020.04.005
32. Davis WA, Zilkens RR, Starkstein SE, et al. Dementia onset, incidence and risk in type 2 diabetes: a matched cohort study with the Fremantle Diabetes Study Phase I. *Diabetologia*. 2017;60(1):89-97. https://doi.org/10.1007/s00125-016-4127-9
33. Callisaya ML, Beare R, Moran C, et al. Type 2 diabetes mellitus, brain atrophy and cognitive decline in older people: a longitudinal study. *Diabetologia*. 2019;62(3):448-458. https://doi.org/10.1007/s00125-018-4778-9
34. Mattson MP, Arumugam TV. Hallmarks of brain aging: adaptive and pathological modification by metabolic states. *Cell Metab.* 2018;27(6):1176-1199. https://doi.org/10.1016/j.cmet.2018.05.011
35. Brooker GJ, Kalloniatis M, Russo VC, et al. Endogenous IGF-1 regulates the neuronal differentiation of adult stem cells. *J Neurosci Res.* 2000;59(3):332-341. https://doi.org/10.1002/(sici)1097-4547(20000201)59:3<332::aid-jnr6>3.0.co;2-2
36. Aberg MA, Aberg ND, Palmer TD, et al. IGF-I has a direct proliferative effect in adult hippocampal progenitor cells. *Mol Cell Neurosci.* 2003;24(1):23-40. https://doi.org/10.1016/s1044-7431(03)00082-4
37. Prozorovski T, Schulze-Topphoff U, Glumm R, et al. Sirt1 contributes critically to the redox-dependent fate of neural progenitors. *Nat Cell Biol.* 2008;10(4):385-394. https://doi.org/10.1038/ncb1700
38. Ma CY, Yao MJ, Zhai QW, et al. SIRT1 suppresses self-renewal of adult hippocampal neural stem cells. *Development.* 2014;141(24):4697-4709. https://doi.org/10.1242/dev.117937

39. Rafalski VA, Brunet A. Energy metabolism in adult neural stem cell fate. *Prog Neurobiol*. 2011;93(2):182-203. https://doi.org/10.1016/j.pneurobio.2010.10.007
40. Kodani N, Nakae J. Tissue-specific metabolic regulation of FOXO-binding protein: FOXO does not act alone. *Cells* 2020;9(3):702. https://doi.org/10.3390/cells9030702
41 Fusco S, Spinelli M, Cocco S, Ripoli C, Mastrodonato A, Natale F, Rinaudo M, Livrizzi G, Grassi C. Maternal insulin resistance multigenerationally impairs synaptic plasticity and memory via gametic mechanisms. *Nat Commun*. 2019 Oct 22;10(1):4799. https://doi.org/10.1038/s41467-019-12793-3
42. Mensà E, Guescini M, Giuliani A, et al. Small extracellular vesicles deliver miR-21 and miR-217 as pro-senescence effectors to endothelial cells. *J Extracell Vesicles* 2020;9(1):1725285. https://doi.org/10.1080/20013078.2020.1725285
43. Yoshida M, Satoh A, Lin JB, et al. Extracellular vesicle-contained eNAMPT delays aging and extends lifespan in mice. *Cell Metab*. 2019;30(2):329342.e5. https://doi.org/10.1016/j.cmet.2019.05.015